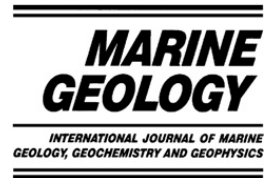




ELSEVIER

Marine Geology 248 (2008) 97–114



www.elsevier.com/locate/margeo

# Sedimentation processes in the Eastern Mediterranean Sea during the Late Glacial and Holocene revealed by end-member modelling of the terrigenous fraction in marine sediments

Y. Hamann<sup>a,\*</sup>, W. Ehrmann<sup>a</sup>, G. Schmiedl<sup>a,1</sup>, S. Krüger<sup>a</sup>, J.-B. Stuut<sup>b</sup>, T. Kuhnt<sup>a</sup>

<sup>a</sup> Institute of Geophysics and Geology, Leipzig University, Talstrasse 35, D-04103 Leipzig, Germany

<sup>b</sup> Research Center Ocean Margins, Bremen University, P.O. Box 330440, D-28334 Bremen, Germany

Received 1 March 2007; received in revised form 2 October 2007; accepted 10 October 2007

## Abstract

We present grain-size distributions of the terrigenous fraction of two sediment cores from the southeast Levantine Sea (SL112) and the northern Aegean Sea (SL148), spanning the time interval from the late glacial to the present. End-member modelling of the grain-size distribution allows discriminating between aeolian and fluvial transport of the sediments and helps to infer palaeoenvironmental conditions in the source areas. Sedimentary and depositional processes during the late glacial and Holocene were controlled by climatic variations of both the northern high latitudes and the African climate system. The sedimentation at site SL112 off Israel is dominated by the suspension load of the River Nile and aeolian dust from the Sahara. Variations in grain size reflect the early to mid-Holocene climate transition from the African Humid Period to recent arid conditions. This climate change was gradual, in contrast to the abrupt humidity change documented in Western Saharan records. This implies a successive decrease in Nile river sediment supply due to a step-wise aridification of the headwaters. The grain-size data of SL112 show a humidity maximum at 5 kyr BP coincident with a regionally-restricted wet phase in the Levantine Sea. The sediments at the North Aegean site SL148 consist of riverine particles and low amounts of aeolian dust, probably derived from South European sources and with probably minor Saharan influence. The sedimentation processes are controlled by climate conditions being characterized by enhanced deposition of dust during the cold and dry glacial period and by decreased aeolian influx during the temperate and humid Holocene.

© 2007 Elsevier B.V. All rights reserved.

*Keywords:* Eastern Mediterranean Sea; grain size; end-member modelling; aeolian dust; river discharge

## 1. Introduction

The Eastern Mediterranean Sea with the Aegean and the Levantine Seas is an intercontinental ocean, semi-

enclosed by land (Fig. 1). It is influenced by different climate regimes. The temperate and humid climate of southeast Europe and Turkey characterizes the northern borderland. In contrast, arid conditions control North Africa and the Near East (Bolle, 2003). The severely different climates find their expression in different types of vegetation, weathering and sediment transport processes. This special setting makes the Eastern Mediterranean Sea a key area for recording past climatic variations of the surrounding land masses.

\* Corresponding author. Fax: +49 341 9732809.

E-mail address: yhamann@rz.uni-leipzig.de (Y. Hamann).

<sup>1</sup> Present address: Institute of Geology and Palaeontology, University of Hamburg, Bundesstrasse 55, D-20146 Hamburg, Germany.



Fig. 1. Map of the Eastern Mediterranean Sea and adjacent areas with locations of sediment cores GeoTü SL112 and GeoTü SL148 marked by black stars. Major rivers and lakes are shown. Black-framed grey arrows indicate major wind systems. Simplified present-day sea-surface circulation is represented by grey elongated arrows (Aksu et al., 1995; Pinardi and Masetti, 2000; Lykousis et al., 2002). 100 m depth contour is given.

Several sedimentological studies have shown that the composition of surface sediments in the Eastern Mediterranean Sea is mainly controlled by the characteristics of the source areas, the climatic conditions on the adjacent continents and the sediment distribution by wind and

ocean currents. Venkatarathnam and Ryan (1971) were among the first who discriminated between different clay mineral assemblages in the Eastern Mediterranean Sea and attributed the abundances of smectite, illite, kaolinite and chlorite to individual source areas. Ehrmann et al.

(2007a) expanded such provenance studies to the Aegean Sea.

Late Quaternary marine sediment records allowed deducing environmental changes and various oceanographic processes, which are tightly linked to climatic variations (e.g. Foucault and Melières, 2000; Gasse, 2000; Mayewski et al., 2004; Robinson et al., 2006, and references therein). A large number of sedimentological, geochemical and faunal studies in the Aegean Sea succeeded to reconstruct the climatic conditions and to document the general trend from cold, glacial climate conditions of the late Pleistocene to the warm, interglacial conditions of the Holocene (e.g. Cramp et al., 1988; Geraga et al., 2000, 2005; Ehrmann et al., 2007b; Kuhnt et al., 2007). In the Levantine Sea, Schilman et al. (2001a, 2001b) used the stable isotope composition of foraminifera in addition to geochemical data on the bulk sediment to reconstruct environmental changes in the hydrological balance of the African continent during the late Holocene. Other palaeoclimatic studies in the Eastern Mediterranean Sea and adjacent areas concentrated on the impact of short-term climate events during the late Quaternary, e.g. Heinrich events, the Younger Dryas, the '8.2 kyr event' and the '4.2 kyr event', which had significant impacts on the depositional regime. These short events have been related to large-scale changes in the world ocean's thermohaline circulation triggered for example by the rapid input of freshwater into the North Atlantic (e.g. Bond et al., 1993; Rohling and Pälike, 2005; Robinson et al., 2006, and references therein) as well regional climatic variations (Cullen et al., 2000; deMenocal, 2001; Migowski et al., 2006). Furthermore, a large number of studies addressed the phenomenon of sapropel formation (e.g. Rohling, 1994, and references therein; Aksu et al., 1995; Rossignol-Strick, 1995; Cramp and O'Sullivan, 1999; Emeis et al., 2000, 2003; Casford et al., 2002, 2003; Meyers, 2006).

The findings from continental records in the Near East are in general agreement with the marine reconstructions and also reflect the long-term trend with intercalated short events (e.g. Bar-Matthews et al., 1999; Felis et al., 2004; Frumkin and Stein, 2004). Lake level reconstructions in the Dead Sea system provided important additional information about the prevailing local humidity and precipitation patterns. Thus, major lake level lowerings reflect an increasing aridity, for example during Heinrich events. Lake level high stands characterize more humid intervals, e.g. during the last glacial (e.g. Neev and Emery, 1995; Bartov et al., 2003).

Despite all these studies, the complex interplay between terrestrial and oceanic processes during late Quaternary climatic changes that left their imprint in the

sediment composition of the Eastern Mediterranean Sea is still poorly understood, because this area is influenced by both northern hemisphere/polar and monsoonal/tropical climate signals. In particular, high-resolution sedimentological studies are rare.

In this paper, we use grain-size distributions to reconstruct sedimentary processes and climatic changes in the region of the Eastern Mediterranean Sea for the last 27 kyr. Especially, we use the method of end-member modelling on the silt fraction. Comparable grain-size records so far are only available in the Western Mediterranean Sea (Moreno et al., 2002). We analyzed two sediment cores from the southeastern Levantine Sea and the northern Aegean Sea (Fig. 1). The cores cover the late glacial and Holocene time intervals in high temporal resolution. The main aims of our study are the understanding of the impact of climate changes on the sedimentation processes and the separation of the prevailing sediment transport mechanisms. Especially we highlight aeolian versus fluvial sediment fluxes and demonstrate differences between the northern and southern realms.

## 2. Environmental setting

### 2.1. Climatic conditions, oceanography and wind systems

The Eastern Mediterranean Sea is situated between two major climatic regimes. The northern and north-western part is governed by the temperate and humid climate of southeast Europe. In contrast, the southern and southeastern part is influenced by the arid conditions of northern Africa, the Arabian Peninsula and the Near East. While the North Atlantic Oscillation (e.g. Hurrell et al., 2003) controls the northern part, the fluctuations of the Intertropical Convergence Zone and the Monsoon/ENSO/Indian Ocean Dipole system influence the southern part (e.g. Schott and McCreary, 2001; Slingo et al., 2002; Saji and Yamagata, 2003).

The surface water of the Eastern Mediterranean Sea generally circulates in an anticlockwise gyre (Fig. 1). It flows parallel to the North African coast towards the east, then turns towards the north and flows along the coast of Israel, Lebanon, Syria to the southern coast of Turkey (e.g. Pinardi and Masetti, 2000). A fraction of this surface water enters the Aegean Sea through several straits of the Hellenic Arc. In the eastern Aegean Sea, it moves to the north and mixes with the cool and low-density Black Sea Water (BSW) entering through the Dardanelles. This water then flows towards the south (Lykousis, 2001), passes the island chain of Greece and enters the Ionian Sea (Fig. 1).

The mean temperature of the Mediterranean surface water (MSW) in the Eastern Mediterranean Sea is 15–27 °C (Wüst, 1960). Its salinity increases steadily during its eastward flow from 38‰ to values >39‰ (Wüst, 1960). Levantine Intermediate Water (LIW) forms south of Turkey during winter by high evaporation and intense convection (Wüst, 1961; Pickard and Emery, 1982). This warm, saline and well-oxygenated water mass flows from 200 to 600 m depth. Eastern Mediterranean Deep Water (EMDW) is formed during winter in the southern Adriatic Sea and the southern Aegean Sea and fills the Ionian and Levantine basins below 800 m (Wüst, 1961; Malanotte-Rizzoli and Hecht, 1988; Klein et al., 1999).

Several dust-bearing winds are relevant for the Eastern Mediterranean region. The Aegean Sea is influenced by the northerly wind system named Etesian in Greece and Meltemi in Turkey (Karalis, 1976; Raicich et al., 2003). The Khamsin influences Egypt and the Near East, blowing from south and southwest. It is associated with particularly intensive dust storms (Stanley and Wingerath, 1996). Furthermore, Scirocco winds from south and southwest carry large volumes of dust and give the air a yellowish color, which is prominent in satellite images (Goudie and Middleton, 2001). Simoon is an important dust-bearing wind in Central and North Africa, which also affects the Mediterranean Sea from the south (Camuffo, 1993). Additionally, Saaroni et al. (1998) described strong easterly winds in Israel, called Sharqiya, which develop over the Near East and bring dust storms to the eastern Levantine Sea.

## 2.2. Sediment supply to the Eastern Mediterranean Sea

The main sediment influx to the Eastern Mediterranean Sea is through rivers. The supply by rivers draining southeast Europe and western Turkey into the Aegean Sea is about  $50 \times 10^6$  t/yr; the suspension load entering the Aegean Sea through the Dardanelles Strait, in contrast, is only ca.  $0.9 \times 10^6$  t/yr (compilation by Ehrmann et al., 2007a). The Seyhan River complex is important for sediment supply from southern Turkey, but is characterized by strong seasonal variations in water discharge

(Shaw, 1978). The small seasonal rivers of the coastal areas of Turkey and Cyprus supply only negligible amounts of sediment. Only a few perennial and some ephemeral rivers in Syria, Lebanon and Israel flow into the Eastern Mediterranean Sea. Their discharge is relatively low. The Yarqon is the most important of these rivers, although with minor importance regarding sediment supply (Fig. 1; Stanley et al., 1997; Sandler and Herut, 2000). Furthermore, Wadi El-Arish draining the Sinai mainly during winter floods provides some sediment (Sandler and Herut, 2000). In the south, the Eastern Mediterranean Sea receives large quantities of sediment by the River Nile. The annual suspension load prior to the construction of the Aswan dam in 1964 was some  $120\text{--}160 \times 10^6$  t/yr (Holeman, 1968; Milliman and Syvitski, 1992; Stanley and Wingerath, 1996), or even  $230 \times 10^6$  t/yr (Garzanti et al., 2006).

The aeolian sediment supply to the Eastern Mediterranean Sea may be as important as the riverine influx in some regions, or may even be the dominant sediment source (Guerzoni et al., 1999). The present aeolian dust influx from Africa was estimated at  $25\text{--}100 \times 10^6$  t/yr to the Eastern Mediterranean and  $80\text{--}120 \times 10^6$  t/yr to Europe (Goudie and Middleton, 2001, and references therein). Annual dust rates of approximately  $30\text{--}60$  g/m<sup>2</sup> have been reported for the southeastern Levantine Sea (Ganor and Foner, 1996; Herut and Krom, 1996). The annual rates for the Aegean Sea are somewhat lower ( $10\text{--}40$  g/m<sup>2</sup>; Nihlen and Olsson, 1995).

## 3. Material and age model

The investigated gravity cores were recovered from the southeastern Levantine Sea off Israel (GeoTü SL112) and the northern Aegean Sea south of Sithonia (GeoTü SL148) during RV Meteor cruise M51/3 in 2001 (Hemleben, 2002; Fig. 1; Table 1). Samples were taken at intervals of 2.5 cm from the upper 3.3 m of core SL148. Core SL112 was sampled in 4 cm intervals to the total length of 5.31 m.

The dominant lithology of the sediment cores is greyish brown to greenish black mud and partly foraminifer-bearing mud with small amounts of sand. The sediments are moderately to strongly bioturbated and have high

Table 1  
Positions of sediment cores recovered during expedition M51/3 and investigated for this study

Core	Latitude	Longitude	Water Depth	Location
GeoTü SL 112	32° 44.52' N	34° 39.02' E	892 m	Israeli Continental Slope
GeoTü SL 148	39° 45.23' N	24° 05.78' E	1094 m	N Aegean Sea, S of Sithonia

The sites are also indicated in Fig. 1.

water contents. Bulk mineralogical analyses show clay minerals, quartz, feldspars, calcite, and minor amounts of amphibole and plagioclase as the key components. The carbonate content is >50% in some intervals of SL112, whereas in SL148 it is generally <25%. The clay fraction consists mainly of illite, kaolinite, smectite, and chlorite in variable concentrations; palygorskite was identified in SL112 throughout the core. Faunal and floral constituents are mainly foraminifera, pteropod fragments, minor amounts of echinoderm fragments, sponge spicules, bivalves, and rare scaphopods, coccoliths, radiolarians, ostracods, and fish remains.

Both sediment cores contain sapropel layer S1, dark olive grey in color. In core SL112, S1 is moderately to faintly laminated. In core SL148, this layer can be subdivided into units S1a and S1b. S1a appears slightly bioturbated, with the bioturbation intensity decreasing downwards. S1b is strongly bioturbated. In core SL148, the Y2-Tephra (Wulf et al., 2002) occurs at a depth of 348 cm, below the analyzed core section. In core SL112, a yet unknown whitish 'S1 tephra' of ca. 1 mm thickness was found within S1 at a depth of 260 cm.

The age model for core SL148 has been taken from Ehrmann et al. (2007b). The age model for core SL112 has been obtained from  $^{14}\text{C}$ -accelerator mass spectrometry (AMS) dating on well-preserved shells of planktonic foraminifera (*G. ruber* white, *G. ruber* pink, *G. sacculifer*, *G. bulloides*, *G. siphonifera*, *O. universa*, *T. quinqueloba*, *N. incompta*). The data were corrected for a reservoir age of 400 years (Siani et al., 2001) and converted to calendar years with the radiocarbon calibration software of Fairbanks et al. (2005). The age

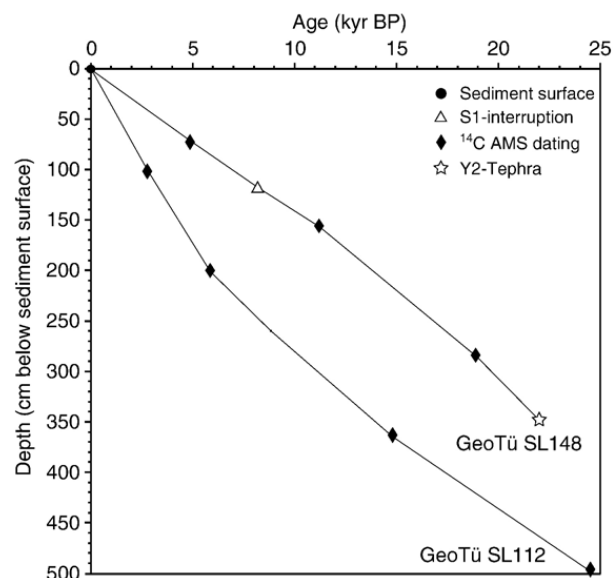


Fig. 2. Depth–age plot for cores GeoTü SL112 and GeoTü SL148. The given age points are listed in Table 2.

models (Table 2; Fig. 2) were calculated by using the AnalySeries software (Paillard et al., 1996).

#### 4. Methods

All samples were freeze-dried and treated with 10% hydrogen peroxide and 10% acetic acid in order to remove organic matter and carbonate, respectively. Then they were sieved through a 63- $\mu\text{m}$  mesh to isolate the sand fraction. The silt and clay fractions were separated by the Atterberg method in settling tubes.

Table 2

Data used for reconstruction the age model for the investigated cores GeoTü SL148 and GeoTü SL112

	Core depth	$^{14}\text{C}$ age	Calendar age	Datum
	(cm)	(kyr BP)	(cal. kyr BP)	
GeoTü SL112	0.00		0.000	Sediment surface
	100.00	3.035 ± 0.030	2.754 ± 0.011	$^{14}\text{C}$ AMS dating
	201.00	5.505 ± 0.030	5.873 ± 0.052	$^{14}\text{C}$ AMS dating
	260.00	8.365 ± 0.065	8.833 ± 0.139	$^{14}\text{C}$ AMS dating
	365.00	12.985 ± 0.060	14.804 ± 0.115	$^{14}\text{C}$ AMS dating
	498.00	20.930 ± 0.130 /- 0.120	24.477 ± 0.185	$^{14}\text{C}$ AMS dating
GeoTü SL148 <sup>a</sup>	0.00		0.000	sediment surface
	71.25	4.750 ± 0.040	4.899 ± 0.057	$^{14}\text{C}$ AMS dating
	117.50		8.200	S1-interruption <sup>b</sup>
	156.25	10.195 ± 0.050	11.217 ± 0.027	$^{14}\text{C}$ AMS dating
	285.00	16.070 ± 0.090	18.878 ± 0.097	$^{14}\text{C}$ AMS dating
	348.00		21.950	Y2-Tephra <sup>c</sup>

<sup>a</sup>Data and the age model for GeoTü SL148 have been taken from Ehrmann et al. (2007b).

<sup>b</sup>Rohling and Pälike (2005).

<sup>c</sup>Wulf et al. (2002).

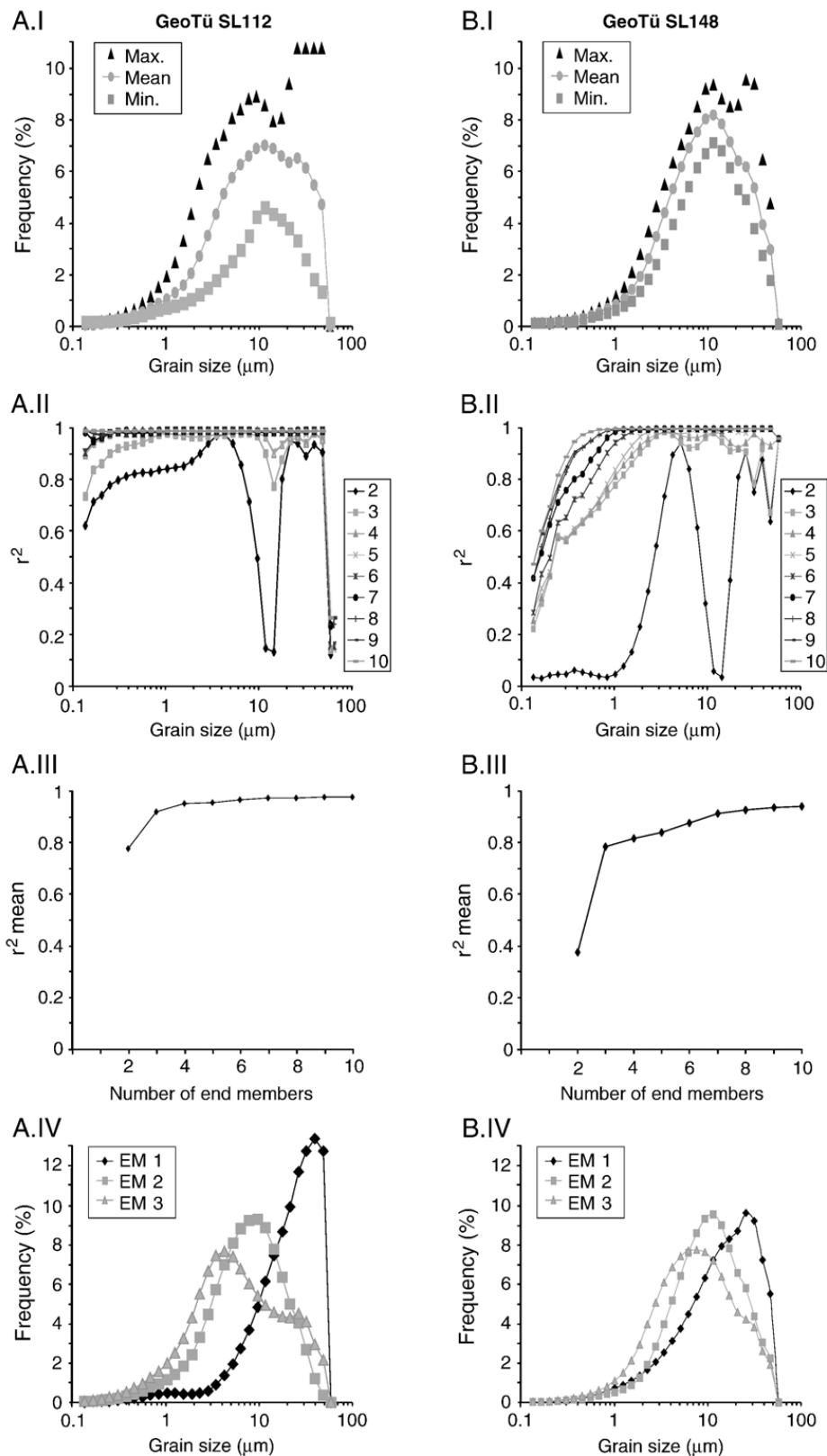


Fig. 3. End-member modelling results of grain-size data of cores GeoTü SL112 (A), and GeoTü SL148 (B). I. Summary statistics of input data (grain-size distributions); maximum, mean and minimum frequency recorded in each size class. II. Coefficients of determination ( $r^2$ ) for each size class of models with 2–10 end-members. III. Mean coefficient of determination ( $r^2$  mean) of all size classes for each end-member model. IV. Grain-size distributions for the three end-member solution.

Grain-size distributions of the carbonate-free silt fraction were measured in 31 size classes in the size range 0–63  $\mu\text{m}$  using a Laser Particle Sizer ‘Analysette 22’ (Fritsch GmbH). We measured each sample four

times and calculated the mean of the measurements for each sample. The standard deviations between the four measurements ranged in core SL112 from 0.051  $\mu\text{m}$  to 0.313  $\mu\text{m}$ , with a mean of 0.143  $\mu\text{m}$ , and in core

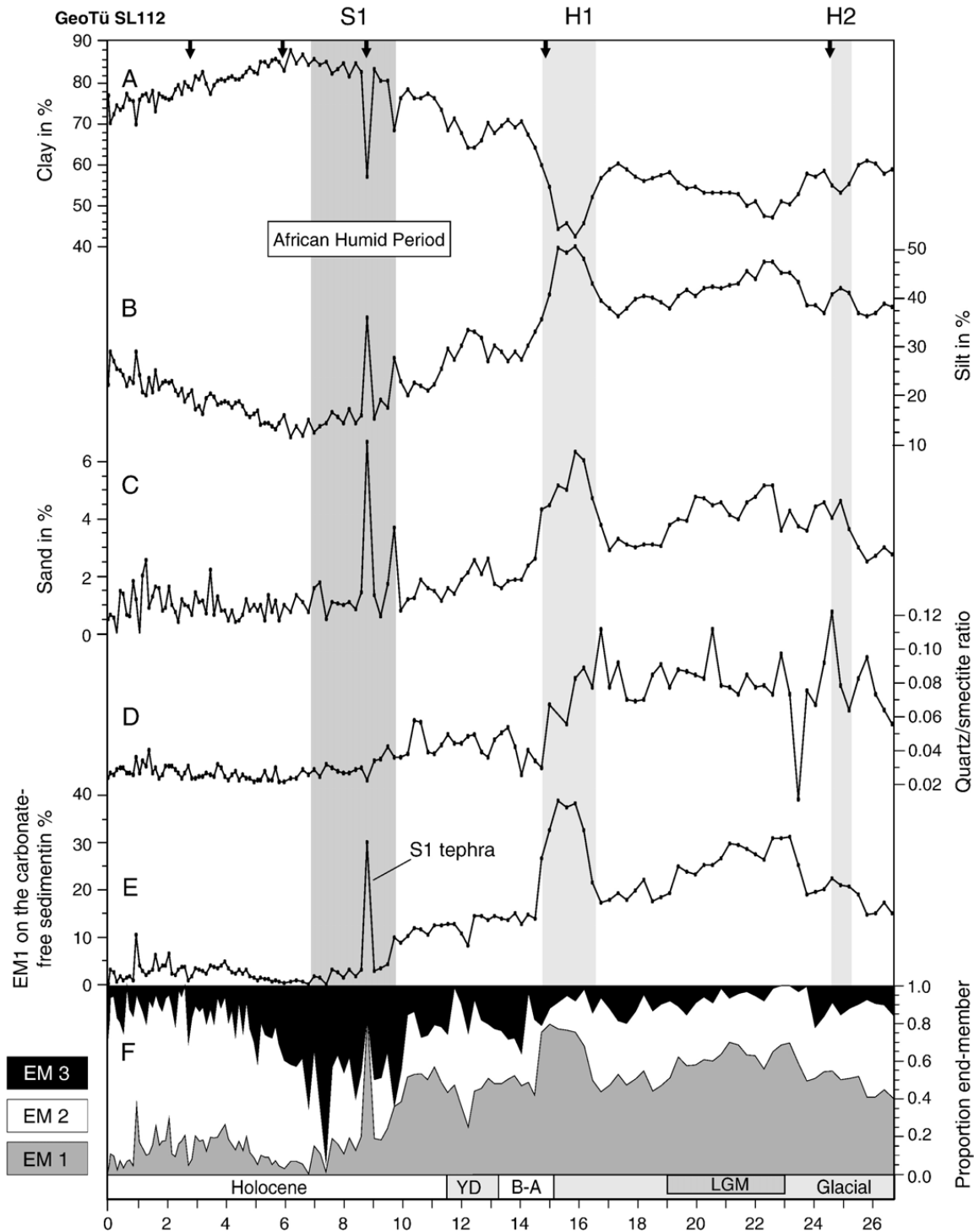


Fig. 4. Sedimentological parameters of GeoTü SL112 (SE Levantine Sea). A) Clay content in %, B) Silt content in %, C) Sand content in %, D) Quartz/smectite ratio, E) Proportions of EM1 on the carbonate-free sediment in %, F) Relative abundance of the three end-members. Dark grey bar indicates sapropel layer S1; light grey bars indicate Heinrich Events H1 and H2. African Humid Period marked after Renssen et al. (2006). Arrows at the top indicate  $^{14}\text{C}$  dates used for constructing the age model of GeoTü SL112 (Table 2, Fig. 2), YD: Younger Dryas, B–A: Bølling–Allerød, LGM: Last Glacial Maximum.

SL148 from 0.046  $\mu\text{m}$  to 0.266  $\mu\text{m}$ , with a mean of 0.134  $\mu\text{m}$ .

We fed our grain-size data into an end-member (EM) model that was generated by Weltje (1997) and can be

used to separate a polymodal dataset into its subpopulations. The coefficients of determination are visualized against grain size for models with 2–10 end-members (Fig. 3A.II, B.II). These coefficients of determination

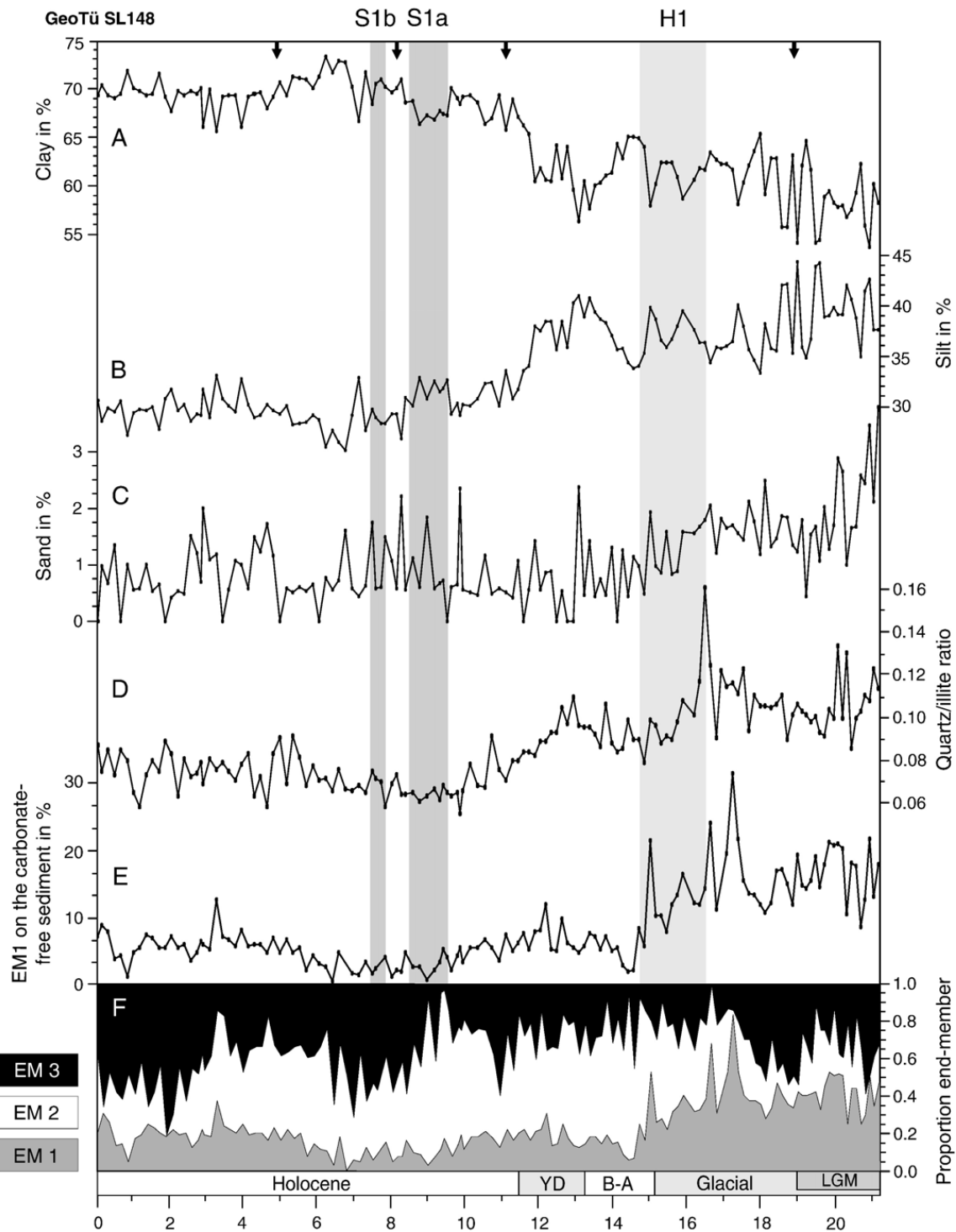


Fig. 5. Sedimentological parameters of GeoTü SL148 (N Aegean Sea). A) Clay content in %, B) Silt content in %, C) Sand content in %, D) Quartz/illite ratio, E) Proportions of EM1 on the carbonate-free sediment in %, F) Relative abundance of the three end-members. Dark grey bars indicate sapropel layers S1a and S1b; light grey bar indicates Heinrich Event H1. Arrows at the top indicate  $^{14}\text{C}$  dates and S1 interruption used for constructing the age model of GeoTü SL148 (Table 2, Fig. 2), YD: Younger Dryas, B–A: Bølling–Allerød, LGM: Last Glacial Maximum.

are calculated to estimate the minimum number of end-members for a satisfactory approximation of the data, calculated from a goodness-of-fit statistics. The coefficients of determination describe the proportion of the variance of each single grain-size class that is reproducible by the approximated values. This proportion is equal to the squared correlation coefficient ( $r^2$ ) of the entered variables and their approximated values (Weltje, 1997). The mean of  $r^2$  of the grain-size classes increases with the number of end-members (Fig. 3 A.III, B.III). The proportion of EM1 on the carbonate-free sediment has been calculated (Figs. 4E and 5E).

For core SL112, we calculated the quartz/smectite ratio. Smectite has been shown to reflect mainly the influx of the Nile (Venkatarathnam and Ryan, 1971; Stanley and Wingerath, 1996), although it may be also present to some degree in Saharan dust (Ganor and Foner, 1996; Goudie and Middleton, 2001). Quartz is an omnipresent sediment component, but is especially enriched in Saharan dust (e.g. Guieu and Thomas, 1996; Goudie and Middleton, 2001; Moreno et al., 2002). Thus, changes in the quartz/smectite ratio may give some indication on aeolian versus fluvial sediment influx. For core SL148, we calculated the quartz/illite ratio with illite indicating terrigenous supply, transported by rivers discharging into the Aegean Sea (Ehrmann et al., 2007a, and references therein).

Illite concentrations have been taken from Ehrmann et al. (2007b) for core SL148, smectite concentrations have been quantified by the same standard method for SL112. Quartz was determined as quartz/ $\text{Al}_2\text{O}_3$  ratio by X-ray analyses of random powder mounts of 1 g ground bulk sediment mixed with 200 mg  $\text{Al}_2\text{O}_3$  as an internal standard.

## 5. Results

All raw data of our sedimentological investigations can be retrieved from the Pangaea data base of the Alfred Wegener Institute at Bremerhaven, Germany ([www.pangaea.de](http://www.pangaea.de)).

The investigated grain-size parameters show distinct temporal variations but also differences between the cores (Figs. 4A–C and 5A–C). Both cores have low terrigenous sand contents and show strong variations in the clay and silt concentrations. The Levantine core SL112 is characterized by sand contents of <6%. The glacial core section is generally coarser than the post-glacial section and has ca. 40% silt and ca. 60% clay. The most pronounced maximum in grain size, with 6% sand, 50% silt and 44% clay, occurs at ca. 16 kyr BP. Above this interval, the grain size decreases step-wise

until ca. 6 kyr BP to <12% silt and >85% clay. Subsequently, the grain size increases again to ca. 30% silt and 70% clay at the sediment surface. The Aegean core SL148 is characterized by sand contents of <3%. The silt contents range from 25% to 45%. They are higher in the 22–12 kyr old glacial sediments (in average 37%) than in the younger part of the core (ca. 30%). The clay concentration increases from ca. 60% in the older part to ca. 70% in the younger part of the core.

In core SL112, the quartz/smectite ratio is higher in the deeper part of the core with variations around 0.08 whereas the upper part shows lower values between 0.02 and 0.03 (Fig. 4D). In core SL148, the quartz/illite ratio range between 0.08 and 0.12 in the deeper part and between 0.06 and 0.08 in the upper part of the core (Fig. 5D).

The average grain-size distribution of the silt fractions in cores SL112 ( $n=133$ ) and SL148 ( $n=137$ ) has a modal grain size near 10  $\mu\text{m}$  (Fig. 3 A.I, B.I). Fig. 3 A.II, B.II show the coefficients of determination plotted against grain size for models with two to ten end-members. In both cores the three-end-member model shows high  $r^2$  for all size classes of the silt fraction ( $r^2_{\text{mean}}=0.92$  in SL112;  $r^2_{\text{mean}}=0.79$  in SL148). The goodness-of-fit statistics show that the three-end-member model for both cores is the best compromise of the number of end-members compared to the coefficients of determination. The grain-size distributions of the end-members of cores are shown in Figs. 3 A.IV, B.IV.

The share of EM1 on the carbonate-free sediment in core SL112 varies from 0 to 40% (Fig. 4E), whereas in core SL148 the amounts are distinctly lower, in general between 0 and 20% (Fig. 5E). The proportional down-core distributions of the end-members of the studied cores are given in Figs. 4F and 5F. The deeper part of core SL112 is dominated by EM3 with values between 0.25 and 0.8. During the upper part, EM3 becomes less important, whereas EM2 rises to 0.4–0.8. EM3 shows highest values between 10.5 and 5.5 kyr BP. In core SL148, EM1 is most abundant in the deeper part of the core, similar to SL112, with a mean value of 0.4. EM1 decreases in the upper part to a mean value of 0.3. EM2 and EM3 show a much more complicated distribution pattern and vary strongly throughout the core.

## 6. Interpretation of the end-member model

The end-member model of Weltje (1997) can be used to identify transport and sedimentation processes from the grain-size distribution of the terrigenous silt fraction. Thus, this algorithm provides a tool to separate the

particle-size distribution into a limited number of subpopulations (Prins et al., 1999) that have been interpreted in terms of variations in bottom current speed and iceberg discharge (Prins et al., 2002), increase of aridity and enhanced wind strength (Stuut et al., 2002), aeolian versus fluvial transported material (Holz et al., 2004). For the particular case of the Western Mediterranean Sea, this technique has been applied by Moreno et al. (2002) sediments of the last glacial period (50–28 kyr BP) in order to discriminate between aeolian input, fine-grained fluvial discharge and a coarser size fraction supplied after torrential rains.

When interpreting the environmental significance of the individual end-members in the cores from the southeastern Levantine Sea and the northern Aegean Sea, we regard the two investigated cores separately, because the end-members are generally influenced by regional atmospheric, oceanographic and sedimentological factors such as, amongst others, nature and distance of sediment source, transport regimes, bottom current strength.

#### 6.1. GeoTü SL112 (southeastern Levantine Sea)

EM1 of the silt fraction in core SL112 has a modal grain size of 40  $\mu\text{m}$  (Fig. 3 A.IV). Comparison with grain sizes of modern aeolian sediments derived from the Sahara provides a strong argument that EM1 can be used as a proxy for aeolian sediment input. Possible dust sources for SL112 are the eastern Libyan Desert, central Algeria, Egypt and Sudan (Fig. 1). Dust sources in the Middle East are of very minor importance. The Saharan dust is transported by the Scirocco and Khamsin (Assallay et al., 1998; Goudie and Middleton, 2001; Engelstaedter et al., 2006). Coudé-Gaussen (1991) and Holz et al. (2004) reported median particle sizes of 5–40  $\mu\text{m}$  and 43  $\mu\text{m}$ , respectively, for North African dust. Saharan dust samples collected in Israel during storms blowing from northern Libya and Egypt consist of 70% silt and 30% clay with a mean in the 20–50  $\mu\text{m}$  size range (Ganor and Mamane, 1982), and a mean silt size of 40  $\mu\text{m}$ , respectively (Ganor and Foner, 1996), i.e. just the size of our EM1. EM1 shows the best sorting of all end-members in core SL112 (Fig. 3 A.IV) that further supports its aeolian origin. In addition, the good correlation in the long-term record of EM1 and the quartz/smectite ratio supports our aeolian interpretation of EM1 based on the fundamentally different input parameters.

Nevertheless, the aeolian interpretation of EM1 has to be considered critically. Processes such as the glacial sea level low stand may affect the grain-size data. In the

Levantine Sea, no major rivers discharged into the basin from the east. Thus, the position of the core site close to the coast could not result in an increased input of fluvial sediment. Also the outflow of the river Nile, at present time the most important sediment source in the southeastern Mediterranean Sea, was reduced (Gasse, 2000). Thus, an aeolian origin of EM1 is more likely.

EM2 of core SL112 has a modal grain size of 10  $\mu\text{m}$ . It has a somewhat poorer sorting than EM1 (Fig. 3 A.IV). Although modal grain sizes of ca. 14  $\mu\text{m}$  were reported from local Israeli loess deposits (Erell and Tsoar, 1999), we do not consider this potential additional dust source to contribute much to EM2. This is because of the dominant proportion of EM2 during the middle and late Holocene, which would suggest an aeolian supply of more than 80% on the carbonate-free sediment. In addition, measurements showed that easterly winds are important, but to a lesser extent than the dominant westerly winds over Israel (Saaroni et al., 1998). Because EM2 comprises most of the present-day and late Holocene silt fraction, we assume that it mainly reflects fluvial sediments derived by the Nile River. Already Venkatarathnam and Ryan (1971) argued, based on clay mineral assemblages in surface sediments, that the smectite-rich Nile suspension load is distributed over a large area of the Eastern Mediterranean Sea and that the sediment off the Israeli coast is dominantly derived from the Nile. In fact, smectite is by far the dominant clay mineral in Holocene sediments of SL112 (Fig. 4D).

EM3 of core SL112 has a modal size of 4  $\mu\text{m}$  (Fig. 3 A.IV), relatively close to EM2. Most likely it also represents fluvial sediment influx, because this grain size correlates well with modern fluvial suspension loads (Walling and Moorehead, 1989). EM3 has the poorest sorting of the three end-members of the core, which supports the interpretation of a fluvial source. It is striking that EM3 has maximum values during the African Humid Period when freshwater input to the Eastern Mediterranean was enhanced (e.g. Rossignol-Strick, 1995; Wehausen and Brumsack, 1999; deMenocal, 2004).

Most of the sediments deposited along the Israeli coast are derived from the Nile and its delta, as could be established by measuring current and wave directions (Emery and Neev, 1960; Golik, 1997) and by various sediment characteristics (e.g. Stanley and Warne, 1998; Sandler and Herut, 2000). Based on  $^{87}\text{Sr}/^{86}\text{Sr}$  studies, Krom et al. (1999) showed that in the region of site SL112, >80% of the surface sediment is derived from the Nile. Also the geochemical analyses of sediments from close to SL112 by Schilman et al. (2001a) confirm that about 70% of the latest Holocene sediment is

composed of Nile particular matter. Our end-member model also suggests that during this time interval the overwhelming part of the terrigenous sediment components are derived by the Nile and that only a minor fraction is Saharan dust.

## 6.2. GeoTü SL148 (northern Aegean Sea)

EM1 of the sediment core SL148 has a median grain size of 24  $\mu\text{m}$  (Fig. 3 B.IV). It is interpreted as wind-derived. The Aegean region is dominated by Etesian winds (Poulos et al., 1997, 2000; Fig. 1). This northerly wind system is active during summer and fall. Etesian winds reach often gale force and probably transport loess southwards. In general, loess has a grain size of 20–50  $\mu\text{m}$  (see compilation of Pye, 1995). Especially, grain-size distributions of southeast European loess formations are characterized by mean sizes of 16–40  $\mu\text{m}$  (Kenig, 2006), and EM1 lies central within this range. An African dust source cannot be excluded, because dust from the Sahara influences the Mediterranean region up to southern and central Europe in minor amounts (e.g. Pye, 1995; Koukouli et al., 2006). Compared to northern sources, dust sources in the south probably provide aeolian sediment to a lesser extent. The correlation of the quartz/illite ratio with EM1 throughout the core supports our aeolian interpretation of EM1.

Also other processes than aeolian origin and transport might have accounted for EM1. The late Quaternary grain-size distribution may have been influenced by changing sea level. During the glacial period, large shelf areas around the North Aegean Sea were exposed because of the lower sea level, and rivers therefore may have delivered coarser material to site SL148. However, the gradual decrease in the concentration of EM1 was already completed at the time of the drastic and step-wise sea level rise to  $-70$  m, which was centred at 14.0 kyr (Bard et al., 1990). The next step-wise rise at ca. 11.5 kyr finds no expression in the silt data. We therefore assume that sea level had no major influence on the silt grain size at site SL148, but may have affected the clay fraction (Ehrmann et al., 2007b).

There is also a possibility that high EM1 proportions resulted from strong bottom-water circulation. Foraminiferal faunas in the Aegean Sea site SL148 show high diversities during the glacial, which has been attributed to high organic matter fluxes and intense deep-water circulation (Kuhnt et al., 2007). This may have enhanced sorting and winnowing of particles. However, the coevally high proportion of the finest grained EM3 during the glacial period argues against this option.

EM2 and EM3 are considerably finer than EM1 and have modal sizes of 11  $\mu\text{m}$  and 7  $\mu\text{m}$ , respectively (Fig. 3 B.IV). Both end-members are probably related to river suspension load. The mode of EM3 is not well defined (Fig. 3 B.IV) and points to a poorly sorted grain-size fraction delivered by rivers. The sediment supply to site SL148 in the North Aegean Sea is dominated by the rivers Strimon, Nestos and Evros, draining the north-eastern European hinterland (Fig. 1).

Within the Aegean Sea, anticlockwise surface currents transport the suspension load to the core position. In addition, based on clay mineralogy Ehrmann et al. (2007a) suggest a possible influence of the Anatolian rivers of West Turkey and minor sediment supply from the Marmara Sea. Core SL148 is influenced in a higher degree by the north Aegean rivers than by the outflow of Marmara Sea and the West Anatolian rivers due to the vicinity of the core position and their much higher sediment discharge of ca.  $17 \times 10^6$  t/year (see compilation Ehrmann et al., 2007a). Therefore, EM2 and EM3 likely represent fluvial material transported depending on the precipitation in the hinterland and related river run-off.

## 7. Discussion

The sedimentation at the investigated sites was dominated by the accumulation of fluvial suspension load. In addition, the sediments contain significant amounts of aeolian dust as indicated by the results of our end-member modelling. The following discussion will concentrate on changes in aeolian versus fluvial sediment supply at the sites in the southeastern Levantine Sea and the northern Aegean Sea during the late Quaternary.

### 7.1. Last Glacial (ca. 27–15 kyr BP)

In core SL112 from the Levantine Sea (Fig. 1), the silt fraction of the glacial sediments between ca. 27 and 15 kyr BP is dominated by EM1, which explains 15–40% of the glacial carbonate-free sediment (Fig. 4E), much more than at any later time. EM2 and EM3 are only of minor importance. Also the other grain-size data show a clear difference between the glacial and the younger sediments. The glacial sediments in average contain 4% sand, 40% silt and 56% clay and they are thus much coarser than modern sediments (Fig. 4A–C). This indicates a strong influence of aeolian sediment influx during the glacial time (Fig. 4F) and accumulation under environmental conditions that were distinctly different from the later ones. The sediment composition probably documents much drier climatic conditions with

enhanced aeolian influx, mainly of silt. Also the enhanced quartz/smectite ratio points to a stronger aeolian influence than today (Fig. 4D). Kohfeld and Harrison (2001) showed that the global glacial dust accumulation from the Sahara/Sahel region was two to five times higher than during the late Holocene.

The glacial sediments of the Aegean Sea core SL148 show a grain-size signature that is very similar to that in the Levantine Sea. The glacial sediments are relatively coarse-grained and contain on average 1–2% sand, 38% silt and 60% clay (Fig. 5A–C). Also here, the silt fraction is dominated by EM1, whereas EM2 and EM3 are much less important. EM1 explains only ca. 15% of the carbonate-free sediment, but this is more than anytime later (Fig. 5E, F). The distribution pattern of EM1 resembles that of the quartz/illite ratio (Fig. 5D, E), which supports our view of a strong impact of wind-transported dust during this time interval. In particular, the glacial termination can be identified by a sharp decrease in EM1 values.

### 7.2. Last Glacial Maximum (ca. 23–19 kyr BP)

Within the glacial interval of SL112, EM1 shows a maximum between 23 and 19 kyr BP, i.e. during the Last Glacial Maximum, and accounts for ca. 30% of the carbonate-free sediment (Fig. 4E, F). In general, the sediments show a coarsening with the presence of up to 5% sand and 48% silt (Fig. 4B, C). The maximum in EM1, the corresponding minima in EM2 and EM3 and the increased deposition of coarse material can be attributed to enhanced aeolian input during the hyper-arid conditions of the Last Glacial Maximum. In addition, because sea level was 120 m lower than today (Bard et al., 1990), the source area for dust expanded. It is assumed that the global atmospheric dust load was up to 10 times higher during the Last Glacial Maximum than during the Holocene (compilation by Goudie and Middleton, 2001). Also in the region of the Eastern Mediterranean Sea, several marine and terrestrial records document an increase in dust supply (e.g. Abed and Yaghan, 2000; Ehrmann et al., 2007b).

In contrast to core SL112, the North Aegean core SL148 shows only indistinctly higher concentration of EM1 during the Last Glacial Maximum (Fig. 5), probably as a result of the complex topography of the region.

### 7.3. Heinrich-equivalent events

The most pronounced excursion in the grain-size data of core SL112 takes place between 17 and 14.5 kyr BP (Fig. 4). The proportion of EM1 almost doubles in this

interval and indicates that some 40% of the carbonate-free sediment is derived by wind (Fig. 4E). EM2 and EM3 are characterized by low values. The sediments become much coarser than before and in average consist of 6% sand, 50% silt and 45% clay (Fig. 4A–C). The change in grain size correlates in time with the Heinrich Event 1. Our data imply particularly dry conditions at the time of Heinrich Event 1 in the source area of the sediments and an even more effective wind transport than during the Last Glacial Maximum. The sediment supply by rivers was low. An equivalent to Heinrich Event 2 is much less evident in core SL112. It is recorded only by slight maxima in the contents of sand (up to 5%) and silt (42%), which are centred at ca. 25 kyr BP (Fig. 4B, C). At about the same time the proportion of EM1 on the carbonate-free sediment somewhat increased from 15% to ca. 20% (Fig. 4E).

During Heinrich Events, freshwater influx to the North Atlantic resulted in temporary restricted oceanic heat transport to the northern high latitudes (Bond et al., 1993; Vidal et al., 1997). Obviously the northern hemisphere climatic events also caused a major environmental change in the Mediterranean Sea region. Based on end-member modelling, Moreno et al. (2002) found evidence for an increase of northward Saharan dust transport into the Western Mediterranean Sea during Heinrich Events. Cacho et al. (2000) showed a correlation of enhanced deep-water ventilation during Heinrich-equivalent events with the increase in northwesterlies over the northwestern Mediterranean Sea. This likely favoured an increase in aeolian influx to the Eastern Mediterranean Sea by stronger Saharan winds. An increased aridity in the Eastern Mediterranean during times of Heinrich Events is further documented by speleothem data and by lake level drops of Lake Lisan/Dead Sea (e.g. Neev and Emery, 1995; Bar-Matthews et al., 1999; Bartov et al., 2003). Both Lake Victoria, source of the White Nile, and Lake Tana, source of the Blue Nile, desiccated (Talbot and Laerdal, 2000; Lamb et al., 2007). The discharge system of the Nile, therefore, must have been strongly reduced, as also indicated by our grain-size data (Fig. 4).

In the North Aegean Sea core SL148 (Fig. 5) a Heinrich-equivalent event 1 is not visible, and Heinrich-equivalent event 2 is outside the investigated core interval. However, Geraga et al. (2000, 2005) documented the impact of the Heinrich Event 1 in the southern and southwestern Aegean Sea. Cold-water planktonic foraminiferal species and pollen data reflect lower sea-surface temperatures and an increase in aridity. Also the palynological studies in the terrestrial record of Tenaghi Phillippon in northeast Greece showed an increased

aridity in southern Europe during times of Heinrich Events (Tzedakis et al., 2003). In contrast, palynological studies of Lake Ioannina in the western part of Greece showed a diminished impact of Heinrich-equivalent events when compared to Western Mediterranean Sea records. This has been attributed to a gradual eastward attenuation of North Atlantic climate signals or, more likely, to local influences of variations in moisture availability (Tzedakis et al., 2002). We therefore assume that the intense cooling during the time of Heinrich Event 1 and the associated intensification of the westerlies or the northeast monsoons did not affect the northernmost Aegean Sea as much as the south Aegean and Levantine Seas and/or that the local climatic conditions masked the signal.

#### 7.4. *Bølling–Allerød (ca. 14 kyr BP)*

At ca. 14 kyr BP, the proportion of EM1 in core SL112 drop back to a level of ca. 0.5, similar to the level during the last glacial (Fig. 4F). The remaining part of the end-member distribution is represented by the fluvial end-members EM2 and EM3. However, because the silt concentration decreased at the same time to ca. 28%, EM1 contributes only 15% to the carbonate-free sediment (Fig. 4E). In contrast, EM3 increased rapidly. The quartz/smectite ratio decreased abruptly (Fig. 4D). Also in core SL148 EM1 decreased at this time and comprised only 5% of the carbonate-free sediment. In contrast, EM2 became more important (Fig. 5E, F). The change in the end-member distribution was accompanied by a fining of the sediment, clearly visible in the decrease of the silt content to 35% and the increase in clay concentrations to 65%. The quartz/illite ratio decreased slightly.

We associate this change in sedimentation both in the Levantine Sea and the Aegean Sea with a decreased aeolian influx and an increased riverine influx of clay-size sediments, related to more humid climate conditions during the Bølling–Allerød period (Neev and Emery, 1995; Severinghaus and Brook, 1999; Bar-Matthews et al., 2003).

#### 7.5. *Younger Dryas (ca. 12 kyr BP)*

The Younger Dryas at ca. 12 kyr BP is expressed in core SL112 by somewhat coarser sediments with up to 2.5% sand and 33% silt (Fig. 4B, C) and a proportion of the aeolian EM1 that is lower than before, but higher than during the Holocene. In the North Aegean core SL148 we observe also a slight increase of the aeolian EM1 and of the quartz/illite ratio.

The Younger Dryas commonly is interpreted as a return towards glacial conditions, with enhanced aridity and an increase in global dust rates (e.g. Bottema, 1995; Gasse, 2000; Kohfeld and Harrison, 2001). However, our end-member data of the Levantine Sea core SL112 seem to contradict this assumption. EM1 accounts for only 10–15% of the carbonate-free sediment and therefore points to a reduction of aeolian dust transport from northern Africa if compared with the glacial time and the time of Heinrich Event 1. No unequivocal records of a dry Younger Dryas were found in North Africa. However, further south, equatorial lake level falls document a drier Younger Dryas (Gasse, 2000). This suggests an African dust source further south, probably activated by the movement of the Subtropical Desert Belt. This source, however, obviously did not affect the Levantine Sea. Also in the Near East a vast spread of deserts with drought and deposition of wind-derived sediments was reported (Rossignol-Strick, 1999; Gvirtzman and Wieder, 2001) and speleothem records of Soreq Cave point to extreme aridity in the Eastern Mediterranean region (Bar-Matthews et al., 2003). However, also this possible aeolian source is not visible in our data. In contrast, in the North Aegean Sea the minor increase in EM1 and the coarsening of sediment suggest slightly more dust supply and a decrease in river supplies of fine-grained sediments and thus a short-term return to cold and dry conditions during the Younger Dryas.

#### 7.6. *Holocene (ca. 11 kyr BP to present)*

The share of EM1 on the silt fraction decreased in core SL112 between ca. 11 and 5.5 kyr BP from 0.75 to 0.50, and its contribution to the carbonate-free sediment decreased from 12% to <5% (Fig. 4E, F). Enhanced EM2 values and maximum EM3 values reflect the general increase of fine-grained sediment particles in the SE Levantine Sea. This fining is also indicated by a gradual decrease in the proportions of sand and silt and an increase of clay (Fig. 4A–C). This grain-size composition can be attributed to enhanced influx through the Nile River. The change in sedimentation patterns documents a gradual climatic change to more humid conditions in North Africa during the African Humid Period (deMenocal et al., 2000; Fig. 4). From 11.5 to 5.5 kyr BP (Renssen et al., 2006), North Africa was dominated by persistently humid conditions (Adamson et al., 1980), visible in a rapid decrease of dust accumulation rates. Thus, deMenocal et al. (2000) estimated a 50% lower dust activity than at present, which can be attributed to the loss of potential dust sources by extensive vegetation

cover (Adamson et al., 1980; Rossignol-Strick, 1999). The enhanced river run-off is well-documented by EM3, but not by EM2. We hypothesize that the maximum in EM3 is related to the deposition of fine-grained sediment due to reduced winnowing as a result of a generally lower bottom-water circulation (Cramp and O'Sullivan, 1999).

It is striking that at the end of the African Humid Period EM3 decreased strongly, whereas EM2 increased at approximately the same extent and EM1 increased only to a much lesser extent (Fig. 4F). The sand content remained low at 0–2%, the silt content increased from ca. 10% at 5.5 kyr BP to ca. 30% at present, and the clay content decreased from 85% to 70% (Fig. 4A–C). The well-known return to arid conditions in northern Africa after the pluvial period (e.g. deMenocal et al., 2000) is not documented by a more pronounced signal of the aeolian versus fluvial end-member signal. Instead, our data indicate that the northern African signal was decoupled from the Nile signal. Obviously the Nile sediment discharge remained high throughout the mid- and late Holocene. This is consistent with relatively high sedimentation rates in the Nile delta after the African Humid Period (Krom et al., 2002). Thus, the enhanced sediment yield of the Nile outflow is probably related to reduced vegetation cover and higher erosional activity, despite a relatively low water discharge.

The gradual change from more humid to more arid conditions of the late Holocene was also reported from the northern Red Sea (Arz et al., 2003). The West African records, in contrast, document abrupt changes (Claussen et al., 1999; deMenocal et al., 2000; Kuhlmann et al., 2004). These regional differences point to a decoupling of the NW African and the NE African climate evolution. Models of the Holocene northern African climate (Renssen et al., 2006) showed differences in the development of precipitation pattern in the Western and the Eastern Sahara, which is associated with different states of vegetation cover. The West Sahara model simulated a green state (up to ca. 7.5 kyr BP), a zone of instability (7.5 to 5.5 kyr BP) and a desert state (5.5 kyr BP to the present). In contrast, the vegetation model of the East Sahara resulted in a more gradual termination, as also seen in our grain-size data of core SL112. In addition, the model showed regions in Egypt and adjacent areas with a vegetation cover of less than 25%. Therefore, possible dust sources were present also during the African Humid Period, which would give a reason for the sedimentation of dust at the beginning of the humid period.

In the North Aegean Sea sediments of core SL148, the concentrations of EM1 throughout the Holocene

reached 5% on average, similar to the rates during the Younger Dryas and the Bølling–Allerød. EM2 and EM3 exhibit a strong variability (Fig. 5F). In general, the sediments are fine-grained with average clay concentrations of ca. 70% in contrast to the glacial interval with mean concentrations of 60% clay. We attribute the lower values of EM1 and the finer grain size to more humid conditions of the Holocene with enhanced supply of suspension load derived by rivers and decreased deposition of dust (Rossignol-Strick, 1999).

Between ca. 9.5 and 5.5 kyr BP, EM1 was characterized by lowest concentrations and accounted for only 2% of the carbonate-free sediment. EM3 had enhanced concentrations. In the same interval the silt content decreased to 26% and the clay content increased to 73% (Fig. 5A–C). The very low quartz/illite ratios correlate with the low EM1 values (Fig. 5D). The data indicate the lowest deposition rate of aeolian sediments throughout the core. A similar situation was documented for the Bølling–Allerød period. This interval reflects more humid and warm conditions during the early to mid-Holocene, coinciding with the African Humid Period in the south and with the formation of sapropel S1 in the Eastern Mediterranean Sea. This climate change is documented in archives from the European continent and adjacent areas (e.g. Rohling, 1994; Rossignol-Strick, 1995, 1999; Emeis et al., 2000). The enhanced concentrations of EM3 are, similar to core SL112, attributed to reduced bottom-water circulation, which favoured the deposition of this small grain size.

At around 1 kyr BP, a short-term decrease of the wind-interpreted EM1 suggests a lowering of aeolian transport. Pollen records in the Near East indicate more humid conditions at 1 kyr BP (Yasuda et al., 2000). After this period, EM1 rose again to levels similar to those of the mid-Holocene dry conditions, coinciding with general strengthened westerlies for the Northern Hemisphere (Mayewski et al., 2004). For the last 600 years, Wick et al. (2003) reported a decrease of woodland in Turkey and attributed this to human activity. This environmental change probably caused an increase in erosion and aeolian transport. For the same time interval, deforestation in southern Europe was also documented in pollen records in the Aegean Sea (Aksu et al., 1995).

## 8. Conclusions

The sedimentological records of sediment cores from the Levantine Sea off Israel and from the Northern Aegean Sea show significantly different patterns between the sites and large temporal variations since the last

glacial. Obviously, the two regions reacted in different ways to the climatic and environmental changes of the late Quaternary.

Although the individual end-members of the silt fraction cannot be interpreted unequivocally, we have strong arguments that the coarse-grained EM1 can be attributed to aeolian transport, whereas the two fine-grained end-members represent fluvial discharge. This interpretation leads to a consistent reconstruction of the climatic evolution in the Eastern Mediterranean borderlands.

Generally, the records in the southeastern Levantine Sea reflect changes in the influx of Saharan dust depending on aridity and wind strength of the North African continent. Fluvial sediments are provided predominantly by the river Nile, depending on the prevailing climatic conditions. In contrast, the Aegean records are influenced by the sediment influx of rivers draining southeast Europe and Turkey. Aeolian sediments are probably reworked from southeast European loess formations, transported by Etesian winds. A Saharan influence is probably negligible.

During the late glacial, both sites show increased influx of aeolian sediments due to drier conditions in the source area and more effective wind transport compared to the Holocene. The proportion of wind-derived sediments is higher in the south eastern Levantine Sea than in the northern Aegean Sea.

Heinrich-equivalent signals are less pronounced in the Eastern Mediterranean when compared to the Western Mediterranean. However, core SL112 provides an unambiguous signal of increased wind intensity during Heinrich Events, especially Heinrich Event 1. In the Aegean Sea core, Heinrich events are not reflected in the sediment record.

After the glacial at ca. 14 kyr BP, both cores provide evidence for changes towards more humid conditions, which we attribute to the Bølling–Allerød period. These changes are reflected by increased depositions of fine-grained sediments, which were deposited by rivers, and by lower values in EM1.

A short-term relapse into cold and dry conditions during the Younger Dryas can only weakly be seen in the southeastern Levantine Sea and the Northern Aegean Sea. It is expressed by a reduced wind-interpreted end-member and coarser grained sediments compared to the Bølling–Allerød before.

The African Humid Period finds expression in the sediments of core SL112 off Israel by increased river supply (EM2, EM3) and decreased dust supply (EM1). This change is clearly reflected by a distinct fining of grain size. The grain-size data and end-member dis-

tribution document a gradual aridification of the North African continent at the end of the African Humid Period in contrast to an abrupt change to arid conditions, reported by several records from northeastern Africa.

## Acknowledgements

The sediment cores were collected by R/V Meteor during M51/3 in 2001. We thank Captain M. Kull and his crew as well as chief scientist C. Hemleben for their help in providing the sediment cores. We thank Y. Milker and S. Dorn for assistance in the laboratories and P.M. Grootes for age determinations. G.J. Weltje is thanked for providing the end-member modelling algorithm. The German Research Council (DFG) financially supported this project. The authors would like to thank two anonymous reviewers for their helpful comments.

## References

- Abed, A.M., Yaghan, R., 2000. On the paleoclimate of Jordan during the last glacial maximum. *Palaeogeogr. Palaeoclimatol. Palaeoecol.* 160, 23–33.
- Adamson, D.A., Gasse, F., Street, F.A., Williams, M.A.J., 1980. Late Quaternary history of the Nile. *Nature* 288, 50–55.
- Aksu, A., Yasar, D., Mudie, P.J., 1995. Paleoclimatic and paleoceanographic conditions leading to development of sapropel layer S1 in the Aegean Sea. *Palaeogeogr. Palaeoclimatol. Palaeoecol.* 116, 71–101.
- Arz, H.W., Lamy, F., Pätzold, J., Müller, P.J., Prins, M., 2003. Mediterranean moisture source for an early-Holocene humid period in the northern Red Sea. *Science* 300, 118–121.
- Assallay, A.M., Rogers, C.D.F., Smalley, I.J., Jefferson, I.F., 1998. Silt: 2–62  $\mu\text{m}$ , 9–4 $\phi$ . *Earth-Sci. Rev.* 45, 61–88.
- Bard, E., Hamelin, B., Fairbanks, R.G., Zindler, A., 1990. Calibration of the  $^{14}\text{C}$  time scale over the last 30,000 years using mass spectrometric U–Th ages from Barbados corals. *Nature* 345, 405–410.
- Bar-Matthews, M., Ayalon, A., Kaufman, A., Wasserburg, G.J., 1999. The Eastern Mediterranean paleoclimate as a reflection of regional events: Soreq cave, Israel. *Earth Planet. Sci. Lett.* 166, 85–95.
- Bar-Matthews, M., Ayalon, A., Gilmour, M., Matthews, A., Hawkesworth, C.J., 2003. Sea-land oxygen isotopic relationships from planktonic foraminifera and speleothems in the Eastern Mediterranean region and their implication for paleorainfall during interglacial intervals. *Geochim. Cosmochim. Acta* 67 (17), 1381–3199.
- Bartov, Y., Goldstein, S.L., Stein, M., Enzel, Y., 2003. Catastrophic arid episodes in the Eastern Mediterranean linked with the North Atlantic Heinrich events. *Geology* 31 (5), 439–442.
- Bolle, H.-J., 2003. *Mediterranean climate. Regional climate studies.* Springer, Berlin. 372 pp.
- Bond, G., Broecker, W.S., Johnsen, S.J., McManus, J.F., Labeyrie, L., Jouzel, J., Bonani, G., 1993. Correlation between climate records from North Atlantic sediments and Greenland ice. *Nature* 365, 143–147.
- Bottema, S., 1995. The Younger Dryas in the Eastern Mediterranean. *Quat. Sci. Rev.* 14, 883–891.
- Cacho, I., Grimalt, J.O., Sierro, F.J., Shackleton, N., Canals, M., 2000. Evidence for enhanced Mediterranean thermohaline circulation during rapid climatic coolings. *Earth Planet. Sci. Lett.* 183, 417–429.

- Camuffo, D., 1993. Controlling the aeolian erosion of the Great Sphinx. *Stud. Conserv.* 38, 198–205.
- Casford, J.S.L., Rohling, E.J., Abu-Zied, R.H., Coole, S., Fontanier, C., Leng, M., Lykousis, V., 2002. Circulation changes and nutrient concentrations in the late Quaternary Aegean Sea: a nonsteady state concept for sapropel formation. *Paleoceanography* 17 (2). doi:10.1029/2000PA000601.
- Casford, J.S.L., Rohling, E.J., Abu-Zied, R.H., Jorissen, F.J., Leng, M., Thomson, J., 2003. A dynamic concept for eastern Mediterranean circulation and oxygenation during sapropel formation. *Palaeogeogr. Palaeoclimatol. Palaeoecol.* 190, 103–119.
- Claussen, M., Kubatzki, C., Brovkin, V., Ganopolski, A., Hoelzmann, P., Pachur, H.-J., 1999. Simulation of an abrupt change in Saharan vegetation in the mid-Holocene. *Geophys. Res. Lett.* 26 (14), 2037–2040.
- Coudé-Gaussen, G., 1991. Les Poussières Sahariennes. John Libbey Eurotext, Mont Rouge France. 485 pp.
- Cramp, A., O'Sullivan, G., 1999. Neogene sapropels in the Mediterranean: a review. *Mar. Geol.* 153, 11–28.
- Cramp, A., Collins, M., West, R., 1988. Late Pleistocene–Holocene sedimentation in the NW Aegean Sea: a palaeoclimatic palaeoceanographic reconstruction. *Palaeogeogr. Palaeoclimatol. Palaeoecol.* 68, 61–77.
- Cullen, H.M., De Menocal, P.B., Hemming, S., Hemming, G., Brown, F.H., Guilderson, T., Sirocko, F., 2000. Climate change and the collapse of the Akkadian empire: evidence from the deep sea. *Geology* 28 (4), 379–382.
- deMenocal, P.B., 2001. Cultural response to climate change during the Late Holocene. *Science* 292, 667–673.
- deMenocal, P.B., 2004. African climate change and faunal evolution during the Pliocene–Pleistocene. *Earth Planet. Sci. Lett.* 220, 3–24.
- deMenocal, P.B., Ortiz, J., Guilderson, T., Adkins, J., Sarnthein, M., Baker, L., Yarusinsky, M., 2000. Abrupt onset and termination of the African Humid Period: rapid climate responses to gradual insolation forcing. *Quat. Sci. Rev.* 19, 347–361.
- Ehrmann, W., Schmiedl, G., Hamann, Y., Kuhnt, T., 2007a. Distribution of clay minerals in surface sediments of the Aegean Sea: a compilation. *Int. J. Earth Sci.* 96, 769–780.
- Ehrmann, W., Schmiedl, G., Hamann, Y., Kuhnt, T., Hemleben, C., Siebel, W., 2007b. Clay minerals in late glacial and Holocene sediments of the northern and southern Aegean Sea. *Palaeogeogr. Palaeoclimatol. Palaeoecol.* 249, 36–57.
- Emeis, K.-C., Sakamoto, T., Wehausen, R., Brumsack, H.-J., 2000. The sapropel record of the eastern Mediterranean Sea — results of Ocean Drilling Program Leg 160. *Palaeogeogr. Palaeoclimatol. Palaeoecol.* 158, 371–395.
- Emeis, K.-C., Schulz, H., Struck, U., Rossignol-Strick, M., Erlenkeuser, H., Howell, M.W., Kroon, D., Mackensen, A., Ishizuka, S., Oba, T., Sakamoto, T., Koizumi, I., 2003. Eastern Mediterranean surface water temperatures and  $\delta^{18}\text{O}$  composition during deposition of sapropels in the late Quaternary. *Paleoceanography* 18 (1), 5–15–18.
- Emery, K.O., Neev, D., 1960. Mediterranean beaches of Israel. *Bull. Geol. Surv. Israel* 26, 1–24.
- Engelstaedter, S., Tegen, I., Washington, R., 2006. North African dust emissions and transport. *Earth-Sci. Rev.* 79, 73–100.
- Erell, E., Tsoar, H., 1999. Spatial variations in the aeolian deposition of dust — the effect of a city: A case study in Be'er Sheva, Israel. *Atmos. Environ.* 33 (24), 4049–4055.
- Fairbanks, R.G., Mortlock, R.A., Chiu, T.-C., Cao, L., Kaplan, A., Guilderson, T.P., Fairbanks, T.W., Bloom, A.L., Grootes, P.M., Nadeau, M.-J., 2005. Radiocarbon calibration curve spanning 0 to 50,000 years BP based on paired  $^{230}\text{Th}/^{234}\text{U}/^{238}\text{U}$  and  $^{14}\text{C}$  dates on pristine corals. *Quat. Sci. Rev.* 24, 1781–1796.
- Felis, T., Lohmann, G., Kuhnert, H., Lorenz, S.J., Scholz, D., Pätzold, J., Al-Rousan, S.A., Al-Moghrabi, S.M., 2004. Increased seasonality in Middle East temperatures during the last interglacial period. *Nature* 429, 164–168.
- Foucault, A., Mélières, F., 2000. Palaeoclimatic cyclicality in central Mediterranean Pliocene sediments: the mineralogical signal. *Palaeogeogr. Palaeoclimatol. Palaeoecol.* 158, 311–323.
- Frumkin, A., Stein, M., 2004. The Sahara-East Mediterranean dust and climate connection revealed by strontium and uranium isotopes in a Jerusalem speleothem. *Earth Planet. Sci. Lett.* 217, 451–464.
- Ganor, E., Mamane, Y., 1982. Transport of Saharan dust across the Eastern Mediterranean. *Atmos. Environ.* 16, 581–587.
- Ganor, E., Foner, H.A., 1996. The mineralogical and chemical properties and the behaviour of aeolian Saharan dust over Israel. In: Guerzoni, S., Chester, R. (Eds.), *The Impact of Desert Dust Across the Mediterranean*. Kluwer Academic Publisher, Dordrecht, pp. 163–172.
- Garzanti, E., Ando, S., Vezzoli, G., Abdel Megid, A.A., El Kammar, A., 2006. Petrology of Nile River sands (Ethiopia and Sudan): sediment budgets and erosion patterns. *Earth Planet. Sci. Lett.* 252, 327–341.
- Gasse, F., 2000. Hydrological changes in the African tropics since the Last Glacial Maximum. *Quat. Sci. Rev.* 19, 189–211.
- Geraga, M., Tsaila-Monopolis, S., Ioakim, C., Papatheodorou, G., Ferentinos, G., 2000. Evaluation of palaeoenvironmental changes during the last 18,000 years in the Myrtoon Basin, SW Aegean Sea. *Palaeogeogr. Palaeoclimatol. Palaeoecol.* 156, 1–17.
- Geraga, M., Tsaila-Monopolis, S., Ioakim, C., Papatheodorou, G., Ferentinos, G., 2005. Short-term climate changes in the southern Aegean Sea over the last 48,000 years. *Palaeogeogr. Palaeoclimatol. Palaeoecol.* 220, 311–332.
- Golik, A., 1997. Dynamics and management of sand along the Israeli coastline, Transformations and evolution of the Mediterranean coastline. *CIESM, Sci. Ser.*, vol. 3, pp. 97–110. Monaco.
- Goudie, A.S., Middleton, N.J., 2001. Saharan dust storms: nature and consequences. *Earth-Sci. Rev.* 56, 179–204.
- Guerzoni, S., Chester, R., Dulac, F., Herut, B., Loye-Pilot, M.-D., Measures, C., Migon, C., Molinaroli, E., Moulin, C., Rossini, P., Saydam, C., Soudine, A., Ziveri, P., 1999. The role of atmospheric deposition in the biochemistry of the Mediterranean Sea. *Prog. Oceanogr.* 44, 147–190.
- Guiu, C., Thomas, A.J., 1996. Saharan aerosols: from the soil to the ocean. In: Guerzoni, S., Chester, R. (Eds.), *The Impact of Desert Dust Across the Mediterranean*. Kluwer Academic Publisher, Dordrecht, pp. 207–216.
- Gvirtzman, G., Wieder, M., 2001. Climate of the last 53,000 years in the eastern Mediterranean, based on soil-sequence stratigraphy in the coastal plain of Israel. *Quat. Sci. Rev.* 20, 1827–1849.
- Hemleben, C., 2002. Short Cruise Report, R.V. Meteor Cruise 51, Leg 3 Valletta-Malta to Istanbul-Turkey 14.11.–10.12.2001.
- Herut, B., Krom, M.D., 1996. Atmospheric input of nutrients and dust to the SE Mediterranean. In: Guerzoni, S., Chester, R. (Eds.), *The Impact of Desert Dust Across the Mediterranean*. Kluwer Academic Publisher, Dordrecht, pp. 349–358.
- Holeman, J.N., 1968. The sediment yield of major rivers of the world. *Water Resour. Res.* 4 (4), 737–747.
- Holz, C., Stuut, J.-B.W., Henrich, R., 2004. Terrigenous sedimentation processes along the continental margin off NW Africa: implications from grain-size analysis of seabed sediments. *Sedimentology* 51, 1145–1154.

- Hurrell, J.W., Kushnir, Y., Ottersen, G., Visbeck, M., 2003. An overview of the North Atlantic Oscillation. *Geophys. Monogr.* 134, 1–35.
- Karalis, J.D., 1976. The turbidity parameters in Athens. *Arch. Meteorol. Geophys. Bioklimatol.*, B (24), 25–34.
- Kenig, K., 2006. Surface microtextures of quartz grains from Vistulian loesses from selected profiles of Poland and some other countries. *Quat. Int.* 152–153, 129–146.
- Klein, B., Roether, W., Manca, B.B., Bregant, D., Beitzel, V., Kovacevic, V., Luchetta, A., 1999. The large deep water transient in the Eastern Mediterranean. *Deep-Sea Res.* I 46, 371–414.
- Kohfeld, K.E., Harrison, S.P., 2001. DIRTMAP: the geological record of dust. *Earth-Sci. Rev.* 54, 81–114.
- Koukoulis, M.E., Balis, D.S., Amiridis, V., Kazadzis, S., Bais, A., Nickovic, S., Torres, O., 2006. Aerosol variability over Thessaloniki using ground based remote sensing observations and the TOMS aerosol index. *Atmos. Environ.* 40 (28), 5367–5378.
- Krom, M.D., Cliff, R.A., Eijssink, L.M., Herut, B., Chester, R., 1999. The characterisation of Saharan dusts and Nile particulate matter in surface sediments from the Levantine basin using Sr isotopes. *Mar. Geol.* 155, 319–330.
- Krom, M.D., Stanley, J.D., Cliff, R.A., Woodward, J.C., 2002. Nile River sediment fluctuations over the past 7000 yr and their key role in sapropel development. *Geology* 30 (1), 71–74.
- Kuhlmann, H., Meggers, H., Freudenthal, T., Wefer, G., 2004. The transition of the monsoonal and N Atlantic climate system off NW Africa during the Holocene. *Geophys. Res. Lett.* 31, 1–4.
- Kuhnt, T., Schmiedl, G., Ehrmann, W., Hamann, Y., Hemleben, C., 2007. Deep-sea ecosystem variability of the Aegean Sea during the past 22 kyr as revealed by benthic foraminifera. *Mar. Micropaleontol.* 64, 141–162.
- Lamb, H.F., Bates, C.R., Coombes, P.V., Marshall, M.H., Umer, M., Davies, S.J., Dejen, E., 2007. Late Pleistocene desiccation of Lake Tana, source of the Blue Nile. *Quat. Sci. Rev.* 26, 287–299.
- Lykousis, V., 2001. Subaqueous bedforms on the Cyclades Plateau (NE Mediterranean) — evidence of Cretan deep water formation. *Cont. Shelf Res.* 21, 495–507.
- Lykousis, V., Chronis, G., Tselepidis, A., Prince, N.B., Theocharis, A., Siokou-Frangou, I., Van Wambeke, F., Donavaro, R., Stavrakakis, S., Duineveld, G., Georgopoulos, D., Ignatiades, L., Souvermezoglou, A., Voutsinou-Taliadouri, F., 2002. Major outputs of the recent multidisciplinary biogeochemical researches undertaken in the Aegean Sea. *J. Mar. Syst.* 33–34, 313–334.
- Malanotte-Rizzoli, P., Hecht, A., 1988. Large-scale properties of the Eastern Mediterranean: a review. *Oceanol. Acta* 11 (4), 323–335.
- Mayewski, P.A., Rohling, E.J., Stager, J.C., Karlén, W., Maasch, K.A., Meeker, L.D., Meyerson, E.A., Gasse, F., van Kreveld, S., Holmgren, K., Lee-Thorp, J., Rosqvist, G., Rack, F., Staubwasser, M., Schneider, R.R., Steig, E.J., 2004. Holocene climate variability. *Quat. Res.* 62, 243–255.
- Meyers, P.A., 2006. Paleoceanographic and paleoclimatic similarities between Mediterranean sapropel and Cretaceous black shales. *Palaeogeogr. Palaeoclimatol. Palaeoecol.* 235, 30–320.
- Migowski, C., Stein, M., Prasad, S., Negendank, J.F.W., Agnon, A., 2006. Holocene climate variability and cultural evolution in the Near East from the Dead Sea sedimentary record. *Quat. Res.* 66, 421–431.
- Milliman, J.D., Syvitski, J.P.M., 1992. Geomorphic/tectonic control of sediment discharge to the ocean: the importance of small mountainous rivers. *J. Geol.* 100, 525–544.
- Moreno, A., Cacho, I., Canals, M., Prins, M.A., Sanchez-Goni, M.-F., Grimalt, J.O., Weltje, G.J., 2002. Saharan dust transport and high-latitude glacial climatic variability: the Alboran Sea record. *Quat. Res.* 58, 318–328.
- Neev, D., Emery, K.O., 1995. *The Destruction of Sodom, Gomorrah, and Jericho: Geological, Climatological, and Archaeological Background.* Oxford University Press, New York. 175 pp.
- Nihlen, T., Olsson, S., 1995. Influence of eolian dust on soil formation in the Aegean area. *Z. Geomorphol.* 39, 341–361.
- Paillard, D., Labeyrie, L., Yiou, P., 1996. Analyseries 1.0: a Macintosh software for the analysis of geographical time-series. *Eos Trans. AGU* 77 (39), 379.
- Pickard, G.L., Emery, W.J., 1982. *Descriptive Physical Oceanography — An Introduction.* Pergamon Press, San Diego. 249 pp.
- Pinardi, N., Masetti, E., 2000. Variability of the large scale general circulation of the Mediterranean Sea from observations and modelling: a review. *Palaeogeogr. Palaeoclimatol. Palaeoecol.* 158, 153–174.
- Poulos, S.E., Drakopoulos, P.G., Collins, M.B., 1997. Seasonal variability in sea surface oceanographic conditions in the Aegean Sea (Eastern Mediterranean): an overview. *J. Mar. Syst.* 13, 225–244.
- Poulos, S.E., Chronis, G.T., Collins, M.B., Lykousis, V., 2000. Thermaikos Gulf Coastal System, NW Aegean Sea: an overview of water/sediment fluxes in relation to air–land–ocean interactions and human activities. *J. Mar. Syst.* 25, 47–76.
- Prins, M., Stuut, J.-B.W., Lamy, F., Weltje, G.J., 1999. End-member modelling of grain-size distributions of deep-sea detrital sediments and its palaeoclimatic significance: examples from the NW Indian, E Atlantic and SE Pacific Oceans. *Geophys. Res. Abstr.* 1, 564.
- Prins, M.A., Bouwer, L.M., Beets, C.J., Troelstra, S.R., Weltje, G.J., Kruk, R.W., Kuijpers, A., Vroon, P.Z., 2002. Ocean circulation and iceberg discharge in the glacial North Atlantic: Inferences from unmixing of sediment size distributions. *Geology* 30 (6), 555–558.
- Pye, K., 1995. The nature, origin and accumulation of loess. *Quat. Sci. Rev.* 14, 653–667.
- Raichich, F., Pinardi, N., Navarra, A., 2003. Teleconnections between Indian monsoon and Sahel rainfall and the Mediterranean. *Int. J. Climatol.* 23 (2), 173–186.
- Renssen, H., Brovkin, V., Fichefet, T., Goosse, H., 2006. Simulation of the Holocene climate evolution in Northern Africa: the termination of the African Humid Period. *Quat. Int.* 150, 95–102.
- Robinson, S.A., Black, S., Sellwood, B.W., Valdes, P.J., 2006. A review of palaeoclimates and palaeoenvironments in the Levant and Eastern Mediterranean from 25,000 to 5000 years BP: setting the environmental background for the evolution of human civilisation. *Quat. Sci. Rev.* 25 (13–14), 1517–1541.
- Rohling, E.J., 1994. Review and new aspects concerning the formation of eastern Mediterranean sapropels. *Mar. Geol.* 122, 1–28.
- Rohling, E.J., Pälike, H., 2005. Centennial-scale climate cooling with a sudden cold event around 8,200 years ago. *Nature* 434, 975–979.
- Rosignol-Strick, M., 1995. Sea–land correlation of pollen records in the Eastern Mediterranean for the glacial–interglacial transition: biostratigraphy versus radiometric time-scale. *Quat. Sci. Rev.* 14, 893–915.
- Rosignol-Strick, M., 1999. The Holocene climatic optimum and pollen records of sapropel 1 in the eastern Mediterranean, 9000–6000 BP. *Quat. Sci. Rev.* 18, 515–530.
- Saaroni, H., Ziv, B., Bitan, A., Alpert, P., 1998. Easterly wind storms over Israel. *Theor. Appl. Climatol.* 59, 61–77.
- Saji, N.H., Yamagata, T., 2003. Indian ocean dipole mode events and African rainfall variability. *CLIVAR Exch.* 27, 1–4.
- Sandler, A., Herut, B., 2000. Composition of clays along the continental shelf off Israel: contribution of the Nile versus local sources. *Mar. Geol.* 167, 339–354.
- Schilman, B., Almogi-Labin, A., Bar-Matthews, M., Labeyrie, L., Paterne, M., Luz, B., 2001a. Long- and short-term carbon

- fluctuations in the Eastern Mediterranean during the late Holocene. *Geology* 29 (12), 1099–1102.
- Schilman, B., Bar-Matthews, M., Almogi-Labin, A., Luz, B., 2001b. Global climate instability reflected by Eastern Mediterranean marine records during the late Holocene. *Palaeogeogr. Palaeoclimatol. Palaeoecol.* 176, 157–176.
- Schott, F.A., McCreary Jr., J.P., 2001. The monsoon circulation of the Indian Ocean. *Prog. Oceanogr.* 51, 1–123.
- Severinghaus, J.P., Brook, E.J., 1999. Abrupt climate change at the end of the last glacial period inferred from trapped air in polar ice. *Science* 286, 930–934.
- Shaw, H.F., 1978. The clay mineralogy of the recent surface sediments from the Cilicia Basin, Northeastern Mediterranean. *Mar. Geol.* 26, 51–58.
- Siani, G., Paterne, M., Michel, E., Sulpizio, R., Sbrana, A., Arnold, M., Haddad, G., 2001. Mediterranean Sea surface radiocarbon reservoir age changes since the last glacial maximum. *Science* 294, 1917–1920.
- Slingo, J., Spencer, H., Hoskins, B., Berrisford, P., Black, E., 2002. The meteorology of the Western Indian Ocean, and the influence of the East African Highlands. *Philos. Trans. R. Soc.* 363, 25–42.
- Stanley, D.J., Wingerath, J.G., 1996. Clay mineral distributions to interpret Nile cell provenance and dispersal: I. Lower River Nile to delta sector. *J. Coast. Res.* 12 (4), 911–929.
- Stanley, D.J., Mart, Y., Nir, Y., 1997. Clay mineral distributions to interpret Nile cell provenance and dispersal: II. Coastal plain from Nile delta to Northern Israel. *J. Coast. Res.* 13 (2), 506–533.
- Stanley, D.J., Warne, A.G., 1998. Nile delta in its destruction phase. *J. Coast. Res.* 14 (3), 794–825.
- Stuut, J.-B.W., Prins, M.A., Schneider, R.R., Weltje, G.J., Jansen, J.H.F., Postma, G., 2002. A 300-kyr record of aridity and wind strength in southwestern Africa: inferences from grain-size distributions of sediments on Walvis Ridge, SE Atlantic. *Mar. Geol.* 180, 221–233.
- Talbot, M.R., Laerdal, T., 2000. The Late Pleistocene–Holocene palaeolimnology of Lake Victoria, East Africa, based upon elemental and isotopic analyses of sedimentary organic matter. *J. Paleolimn.* 23, 141–164.
- Tzedakis, P.C., Lawson, I.T., Frogley, M.R., Hewitt, G., Preece, R., 2002. Buffered tree population changes in a Quaternary refugium: evolutionary implications. *Science* 297, 2044–2047.
- Tzedakis, P.C., McManus, J.F., Hooghiemstra, H., Oppo, D.W., Wijnstra, T.A., 2003. Comparison of changes in vegetation in northeast Greece with records of climate variability on orbital and suborbital frequencies over the last 450 000 years. *Earth Planet. Sci. Lett.* 212, 197–212.
- Venkatarathnam, K., Ryan, W.B.F., 1971. Dispersal patterns of clay minerals in the sediments of the eastern Mediterranean Sea. *Mar. Geol.* 11, 261–282.
- Vidal, L., Labeyrie, L., Cortijo, E., Arnold, M., Duplessy, J.C., Michel, E., Becqué, S., van Weering, T.C.E., 1997. Evidence for changes in the North Atlantic Deep Water linked to meltwater surges during the Heinrich events. *Earth Planet. Sci. Lett.* 146, 13–27.
- Walling, D.E., Moorehead, R.W., 1989. The particle size characteristics of fluvial suspended sediment: an overview. *Hydrobiologia* 176/177, 125–149.
- Wehausen, R., Brumsack, H.-J., 1999. Cyclic variations in the chemical composition of eastern Mediterranean Pliocene sediments: a key for understanding sapropel formations. *Mar. Geol.* 153, 161–176.
- Weltje, G.J., 1997. End-member modelling of compositional data: Numerical–statistical algorithms for solving the explicit mixing problem. *Jour. Math. Geol.* 29, 503–549.
- Wick, L., Lemcke, G., Sturm, M., 2003. Evidence of Lateglacial and Holocene climatic changes and human impact in eastern Anatolia: high-resolution pollen, charcoal, isotopic and geochemical records from the laminated sediments of Lake Van, Turkey. *Holocene* 13 (5), 665–675.
- Wulf, S., Kraml, M., Kuhn, T., Schwarz, M., Inthorn, M., Keller, J., Kuscu, I., Halbach, P., 2002. Marine tephra from the Cape Riva eruption (22 ka) of Santorini in the Sea of Marmara. *Mar. Geol.* 183, 131–141.
- Wüst, G., 1960. Die Tiefenzirkulation des Mittelländischen Meeres in den Kernschichten des Zwischen- und des Tiefenwassers. *Dtsch. Hydrogr. Z.* 13 (3), 105–131.
- Wüst, G., 1961. On the vertical circulation of the Mediterranean Sea. *J. Geophys. Res.* 66 (10), 3261–3271.
- Yasuda, Y., Kitagawa, H., Nakagawa, T., 2000. The earliest record of major anthropogenic deforestation in the Ghab Valley, northwest Syria: a palynological study. *Quat. Int.* 73/74, 127–136.